Miniature Piezoelectric Mobile Robot driven by Standing Wave

H. H. Hariri G. S. Soh* S. H. Foong K. L. Wood K. Otto
Temasek Laboratories
Singapore University of Technology and Design
Singapore

Abstract— *In this paper, we will study the locomotion behaviour of a meso scale legged piezoelectric mobile robot driven by standing wave. The design exploits the use of standing waves to be transmitted to its legs to propel the robot forward. A piezoelectric robot is designed and discussion are provided regarding the dynamic modelling of the mobile robot. An experimental measure of the speed according to the applied voltage is given herein on acrylic substrate. We have shown that 50 mm by 10 mm piezo actuator have demonstrated a bi-directional walking speed on acrylic substrate of up to 4 cm/s when a 40 V voltage is applied.*

Keywords: piezoelectric, locomotion, standing wave, mobile robot

I. Introduction

Piezoelectric actuators are a potential enabling technology for autonomous micro robots with locomotion abilities rivalling biological systems. Many piezoelectric miniature robots on a solid substrate can be found in literature [1–7]. A review on the locomotion principles for piezoelectric mobile miniature robot can be found in [8]. The locomotion principle used in this paper differs from those presented and is based on standing wave generation to create bi-directional motion, as inspired from piezoelectric ultrasonic linear motors. An overview of piezoelectric ultrasonic motors can be found in [9]. The first bi-directional linearly motion standing wave ultrasonic linear motor was reported by [10]. The motor consists of a rectangular metal-piezoceramic composite thin plate with three teeth. Eight piezoelectric patches are used over the entire length of the rectangular metal plate and therefore eight input voltages is required. The fundamental principle of this linear motor is such that teeth on the right side of a standing wave crests generate right diagonal thrust force as thetooth is pressed against the slider. Similarly, teeth on the left side of the wave crests will create left diagonal thrust force to move the slider left. The motor used the third and fourth bending mode to generate bi-directional motion.

Another type of ultrasonic linear motor that uses standing wave principle is reported in [11]. The motor consists of a metallic plate and two piezocermaic plates bonded to the metallic plate. Each piezoceramic plate is composed of small piezoelectric patches with alternate polarity reversals which leads to complex fabrication process. This motor use only the fourth bending vibration mode and the direction of motion is controlled by phase difference between the applied electric signals at the PZT plates.

The bi-directional driving principle reported in [10] had been used in [12] for mobile robotic application. Their robot consists of a rectangular metal-piezoceramic composite thin plate with three legs. Six piezoelectric patches are used over the entire length of the rectangular metal plate to create the third and fourth bending mode to generate bi-directional motion. In this paper, we explored a new design of a piezoelectric mobile robot, which built upon the principle of ultrasonic motors as reported by [10] and [12]. Our architecture consists of a single piezoelectric patch and uses the first and third bending mode to generate bi-directional motion. This has the advantage of decreasing the manufacturing complexity due to lesser wires and required input voltage and is our first step in make such system truly autonomous.

In the following, we will introduce the operation principle of our piezoelectric mobile robot. Next, we determine the required operating frequencies and the legs positions for the piezoelectric mobile robot to generate the first and the third bending modes for locomotion. Subsequently, the design and fabrication process of the piezoelectric mobile robot is presented. Finally, experimental verification is shown where we measure the speed of the robot as it travels on an acrylic substrate according to the voltage applied.

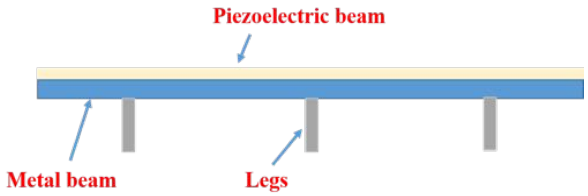

Fig. 1. Robot Structure: piezoelectric unimorph actuator with attached legs

II. Operation principle of the robot

The operation of our piezoelectric robot is based off an unimorph actuator. A unimorph actuator consists of one active material and one passive material bonded together. When the active layer is driven to expand or contract, the

*sohgimsong@sutd.edu.sg

passive layer resists this change by elongating and bending due to the difference in strain properties between these two layers. Thus, when using piezoelectric ceramic material such as PZT as an active layer in a unimorph actuator, controllable up and down bending of the passive layer can be achieved by simply changing the direction of the applied electric field to create relative motion between two bodies.

Our piezoelectric mobile robot consists of a piezoelectric unimorph actuator with legs attached as shown in Figure 1. The piezoelectric unimorph actuator, which is an asymmetric structure with one ceramic layer bonded to an elastic layer, is responsible for its motion and it is characterized by two energy transformations. The first transformation reflects the reverse piezoelectric effect, which generates small motion of mobile miniature robots. The second transformation contains specific locomotion principles, which amplifies the motion of the piezoelectric mobile robot.

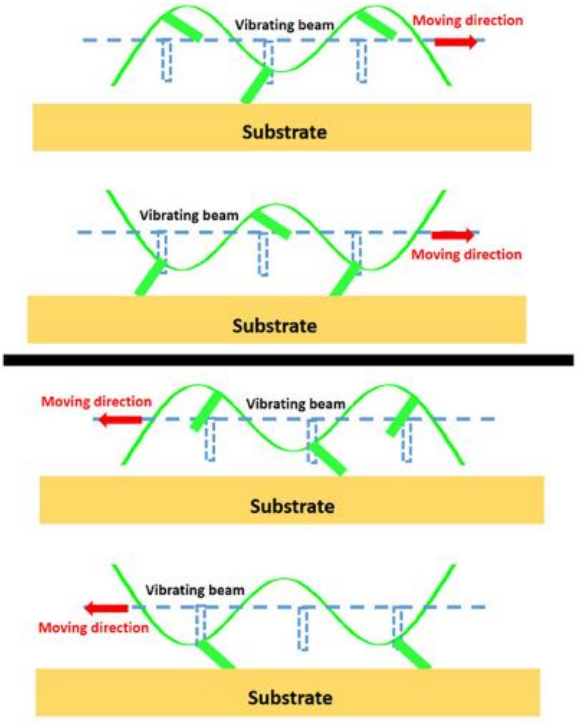

Fig. 2. Locomotion Principle

Figure 2 gives an overview of our locomotion principle. It uses standing wave generated by the piezoelectric beam to create forward and backward motion. The motion direction of the robot is dependent on how the legs are placed and the modal shape of the piezoelectric beam. The general idea is that if stimulated at the appropriate beam bending mode, legs located to the left of each antinodes produces motion that moves the robot towards the right, and legs located to the right of each antinodes moves the robot to the left due to friction. To achieve this locomotion behavior, the legs should be placed such that it falls on the left of the antinodes for one modal shape and vice versa at another modal shape. Hence, by applying appropriate sinusoidal voltage on the piezoelectric beam, one is able to control the modes shapes of the standing wave to generate bi-directional motion. Note that, on requirement is that the legs should always be perpendicular to the contour of the standing wave at the points of attachments. Therefore, the stiffness of the chosen material for the legs should be sufficiently higher than the equivalent stiffness of the piezoelectric unimorph actuator.

III. Modeling of the piezoelectric unimorph actuator

In order to determine the operating frequencies and the legs positions for the piezoelectric mobile robot at the two selected bending modes of operation, the dynamic equation of motion for the piezoelectric unimorph actuator needs to be determined to obtain for its resonance frequencies and associated modal shapes.

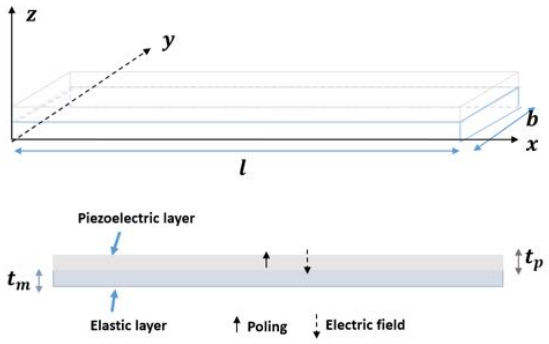

Fig. 3. Geometric parameters for the piezoelectric unimorph actuator

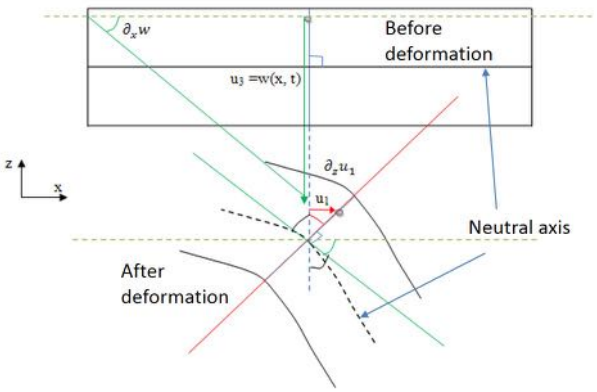

Fig. 4. Kinematics of the deformation of an Euler-Bernoulli beam

A. *Equation of motion of the piezoelectric unimorph actuator*

The dynamic equation of motion for a piezoelectric unimorph actuator as shown in Figure 3, in the transverse direction was derived previously based on Euler-Bernoulli

hypothesis [13] and was found to be

$$(cI)_{eq}\frac{\partial^4 w(x,t)}{\partial x^4} + (\rho A)_{eq}\frac{\partial^2 w(x,t)}{\partial t^2} = -e_p \partial_x^2 E_3(x,t) b \int_{t_m}^{t_m+t_p} (z - z_n). \quad (1)$$

z_n is the neutral axis computed from the bottom of the system and $w(x,t)$ denotes the transverse displacement of the neutral axis of the piezoelectric unimorph actuator as shown in Figure 4. $(cI)_{eq}$ and $(\rho A)_{eq}$ are the equivalent flexural rigidity and the equivalent mass per unit length of the piezoelectric unimorph actuator as defined by

$$(cI)_{eq} = (I_p c_p + I_m c_m), \quad (2)$$
$$(\rho A)_{eq} = b(\rho_p t_p + \rho_m t_m), \quad (3)$$

where ρ_p and ρ_m are the volume densities for the piezoelectric and elastic layers respectively and $I_m = b\int_0^{t_m}(z - z_n)^2\,\mathrm{dz}$ and $I_p = b\int_{t_m}^{t_m+t_p}(z - z_n)^2\,\mathrm{dz}$.

The neutral axis z_n can be calculated by setting the sum of all forces in x-direction over the entire cross-section to zero [14]:

$$\int_0^{t_m+t_p} F_x \mathrm{dA} = 0. \quad (4)$$

This yields

$$\int_0^{t_m} \sigma_1^m(z)\,\mathrm{dz} + \int_{\mathrm{t_m}}^{\mathrm{t_m+t_p}} \sigma_1^{\mathrm{p}}(\mathrm{z})\,\mathrm{dz} = 0. \quad (5)$$

σ_1^p and σ_1^m are referred to as stresses induced in the piezoelectric and elastic layers respectively. These stresses can be obtained using Hooke's law and superposition,

$$\sigma_1^m = c_m \varepsilon_1, \quad (6)$$
$$\sigma_1^p = c_p \varepsilon_1 - e_p E_3 = \frac{1}{s_{11}^E}\varepsilon_1 - \frac{d_{31}}{s_{11}^E}E_3, \quad (7)$$

where c_m, s_{11}^E and d_{31} are the Young modulus for the elastic layer, the elastic compliance for the piezoelectric layer and piezoelectric constant for the piezoelectric layer respectively. E_3 denotes the applied electric field direction and in this case is in the z direction.

Substituting equation (6) and (7) into (5) gives,

$$\int_0^{t_m} c_m(z - z_n)\,\mathrm{dz} + \int_{\mathrm{t_m}}^{\mathrm{t_m+t_p}} \mathrm{c_p}(\mathrm{z} - \mathrm{z_n})\,\mathrm{dz} = 0, \quad (8)$$

and upon simplifying yields the neutral axis z_n,

$$z_n = \frac{1}{2}\frac{c_m t_m^2 + c_p t_p^2 + 2c_p t_p t_m}{c_m t_m + c_p t_p}. \quad (9)$$

B. Resonance frequencies and mode shapes for free-free piezoelectric unimorph actuator

The solution to transverse displacement of the unimorph actuator can be obtained by solving the dynamic equation (1) using the separation of variables method. By letting

$$w(x,t) = \phi(x)\gamma(t) = \phi(x)\gamma_0 e^{j2\pi f t}, \quad (10)$$

and ignoring the second member, equation (1) can be reformulated as

$$\frac{d^4\phi(x)}{dx^4} - \beta^4\phi(x) = 0, \quad (11)$$

where β denotes the wavenumber [14] and is related to the resonance frequency f such that

$$\beta^4 = (2\pi f)^2\frac{(\rho A)_{eq}}{(cI)_{eq}}. \quad (12)$$

The solution to equation (11), which denotes the mode shape of the beam $\phi(x)$, yields the general form

$$\phi(x) = A\sin(\beta x) + B\cos(\beta x) + C\sinh(\beta x) + D\cosh(\beta x), \quad (13)$$

and for a free-free piezoelectric unimorph actuator, its boundary conditions are govern by

$$\partial_x^2 w|_{x=0} = \partial_x^2 w|_{x=l} = \partial_x^3 w|_{x=0} = \partial_x^3 w|_{x=l} = 0. \quad (14)$$

Hence, by applying (14) to equation (13), yields the following homogenous system

$$\begin{bmatrix} 0 & -1 & 0 & 1 \\ -1 & 0 & 1 & 0 \\ -\sin(\beta l) & -\cos(\beta l) & \sinh(\beta l) & \cosh(\beta l) \\ -\cos(\beta l) & \sin(\beta l) & \cosh(\beta l) & \sinh(\beta l) \end{bmatrix} \begin{bmatrix} A \\ B \\ C \\ D \end{bmatrix} = \begin{bmatrix} 0 \\ 0 \\ 0 \\ 0 \end{bmatrix}. \quad (15)$$

To ensure that no trivial solution exists, we solve for values of βl that result in the determinant

$$\begin{Vmatrix} 0 & -1 & 0 & 1 \\ -1 & 0 & 1 & 0 \\ -\sin(\beta l) & -\cos(\beta l) & \sinh(\beta l) & \cosh(\beta l) \\ -\cos(\beta l) & \sin(\beta l) & \cosh(\beta l) & \sinh(\beta l) \end{Vmatrix} = 0. \quad (16)$$

This is equivalent to solving the characteristic equation of the system [14],

$$1 - \cos(\beta l)\cosh(\beta l) = 0. \quad (17)$$

Notice that there is no closed form solution to this equation, and the solution needs to be computed numerically. The first ten solutions to the characteristic equation (17) are listed in Table I.

Using Table I, the natural frequencies for the piezoelectric unimorph actuator can be determined from equation (12) as

$$f_n = \frac{(\beta_n l)^2}{2\pi l^2}\sqrt{\frac{(cI)_{eq}}{(\rho A)_{eq}}} \quad (18)$$

n	1	2	3	4	5
$\beta_n l$	4.73	7.85	10.99	14.14	17.28
n	6	7	8	9	10
$\beta_n l$	20.42	23.56	26.7	29.85	33

TABLE I. Solution of the characteristic equation for free-free piezoelectric unimorph actuator

The mode shapes $\phi_n(x)$ can be determined by solving equation (15), this yields

$$\phi_n(x) = A_n \varphi_n(x) \tag{19}$$

where

$$\varphi_n(x) = \sin(\beta_n x) + \sinh(\beta_n x) - \frac{\sin(\beta_n l) - \sinh(\beta_n l)}{\cos(\beta_n l) - \cosh(\beta_n l)}(\cos(\beta_n x) + \cosh(\beta_n x)). \tag{20}$$

and

$$A_n^2 = \frac{1}{(\rho A)_{eq} \int_0^l \varphi_n(x)^2 \, \mathrm{dx}}. \tag{21}$$

IV. Design and fabrication of the piezoelectric mobile robot

In this section, we described the design process of our piezoelectric mobile robot and how it was fabricated.

A. Design

The design process begins by choosing the geometric parameters of the robot based on the dimensions of commercially available piezoelectric layers. In our case, the NCE53, soft PZT from Noliac Inc. was chosen to be the active layer of the unimorph actuator due to the size range that we are looking at. Its dimensions are as shown in Table II. Next, Aluminum was chosen as the passive layer of the unimorph actuator due to its efficient electromechanical conversion. Both the PZT and Aluminum have similar dimensions except for thickness, where it was chosen differently to obtain the maximum electromechanical conversion from the piezoelectric material as a composite structure.

The thickness ratio for optimal electromechanical conversion for aluminum as the passive layer [15] in this case was found to be

$$\frac{t_p}{t_m} = 0.54. \tag{22}$$

Hence, the aluminum thickness t_m was chosen to be 0.926 mm for the selected PZT layer. However, 1 mm thick aluminum sheet was used instead because of its commercial availability.

Next, we solve equation (18) and (19) to determine the operating frequencies and the leg positions of the piezoelectric mobile robot. As we are interested in bi-directional motion using the same leg, two operating frequencies are required, with each frequency moving the robot in a particular direction. We chose to work with the first and third resonant frequency (f_1, f_3) because of symmetry reasons and lower power consumption if operated at lower frequency. Using equation (18) and Table I, the two resonant frequencies are found to be 2.41 kHz and 12.77 kHz.

Properties, geometry	$PZT(p)$	Aluminium (m)
$c_m(Pa)$	-	69×10^9
$\rho_p, \rho_m(kg.m^{-3})$	7600	2700
$d_{31}(m.V^{-1})$	-1.5×10^{-10}	-
$S_{11}(Pa^{-1})$	1.6×10^{-11}	-
$l_p, l_m \times b \times t_p, t_m(mm^3)$	$50 \times 10 \times 0.5$	$50 \times 10 \times 1$

TABLE II. Properties and geometry of the PZT and the aluminium layer

	Legs positions (mm)
Leg 1	14.4
Leg 2	24.7
Leg 3	41.7

TABLE III. Legs positions at f_1 and f_3

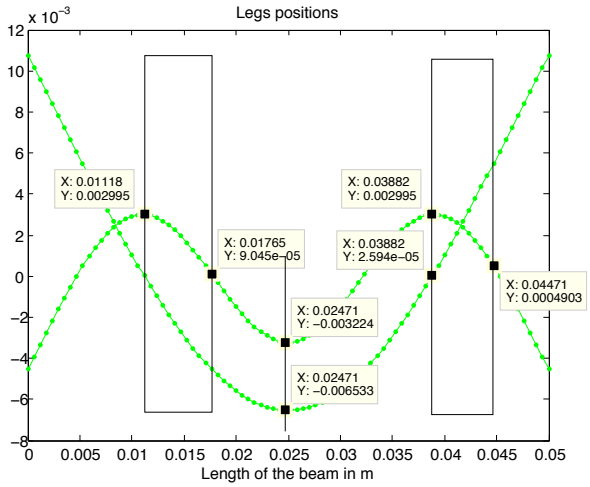

Fig. 5. Mode shapes and legs positions at f_1 and f_3

Next, we determine the legs positions along the unimorph actuator. They can be synthesized from the corresponding mode shapes as described by equation (19). Figure 5 shows the model shape $\phi_m(x)$ for the first and third resonant frequency. Using the antinodes and horizontal axis as a guide, two regions as shown by the rectangles can be identified where the displacement of the beam falls on the left of the antinodes in the first mode shape, and falls on the right in the third mode shape. The legs can be placed anywhere between the rectangles. We chose to place at the center for each of these rectangles and the leg positions are given in Table III. Notice that and additional leg 2 is added at the antinode of the first and the third mode shape. It doesn't affect the motion of the robot but increases its stability.

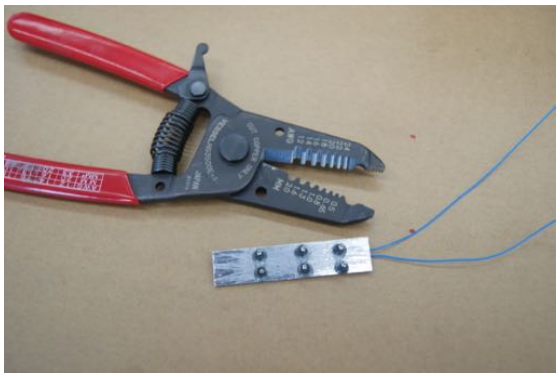

Fig. 6. Legs positions on the aluminium beam

B. Fabrication

The final piezoelectric robot has six cylindrical shaped steel legs bonded onto the aluminium beam using a strong bonding epoxy adhesive (two parts Araldite epoxy) at the appropriate positions given in Table III. It is as shown Figure 6. Next, the piezoelectric layer is bonded onto the aluminum layer using the same epoxy. The piezoelectric layer is a wraparound electrode in order to have both electrodes on the same face. At the end, thin wires are soldering on the PZT electrodes. Figure 7 shows the complete prototype with an embedded mass to increase its frictional contact.

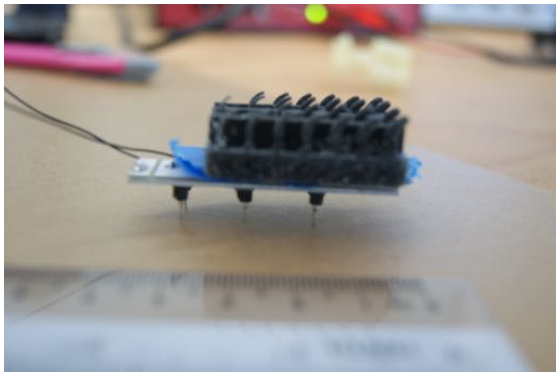

Fig. 7. Prototype of the piezoelectric robot with an embedded mass

V. Experiments

In this section, experiments are conducted to quantify the performance of the piezoelectric robot. The objective is to correlate its locomotion speed given an input voltage, as well as to show that it can work in practical settings.

Sinusoidal voltage are generated by a function generator and amplified via a piezoelectric driver to the PZT layer. The robot was found to moves at an applied frequency of 2.6 kHz and 12.7 kHz, which are consistent with the calculated analytical frequencies of 2.41 kHz and 12.77 kHz. The 2.6 kHz corresponds to the first vibration mode where the robot moves forward and the 12.7 kHz corresponds to the third vibration mode where the robot moves backward. The speed of the robot is calculated by the formula $\frac{d}{t}$ where d is taken equal to $30cm$ and t is measured by a chronometer for different applied voltages at both frequencies. Four measurements are taken for each applied voltage and the average is calculated. They are as shown in Tables IV and V. Figure 8 show the average velocity of the piezoelectric robot on an acrylic substrate for each applied voltage. An image sequence of the piezoelectric robot moving on a substrate is shown in Figure 9

Voltage (V)	Trail (1)	Trail (2)	Trail (3)	Trail (4)	Average (s)
20	15.74	15.12	19.3	15.3	16.36
40	8.24	7	8.32	7.2	7.69
60	6.56	6.06	6.14	5.56	5.83
80	4.38	4.26	4.88	4.7	4.55
100	4.3	4	4.14	3.88	4.08

TABLE IV. Time spent in s for $30cm$ distance at $2.6kHz$

Voltage (V)	Trail (1)	Trail (2)	Trail (3)	Trail (4)	Average (s)
20	0	0	0	0	0
40	9.56	7.64	7.7	7.56	8.12
60	5.24	6	5.68	5.5	5.6
80	3.94	4.06	4.32	4.24	4.14
100	3.62	3.56	3.5	3.74	3.6

TABLE V. Time spent in s for $30cm$ distance at $12.7kHz$

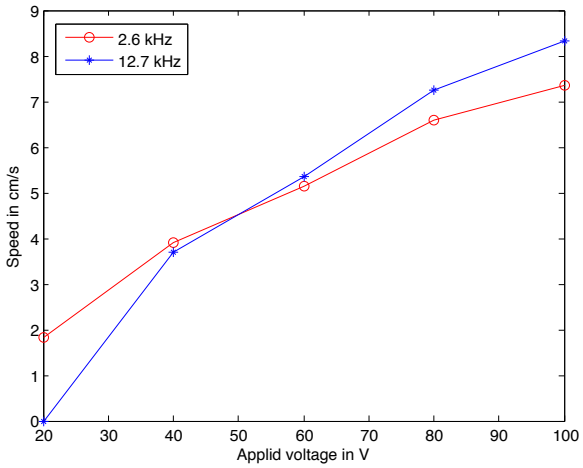

Fig. 8. Speed versus applied voltage on acrylic substrate

VI. Conclusion

The locomotion behaviour of a meso scale legged piezoelectric mobile robot driven by standing wave is presented in this paper. The robot consists of a piezoelectric unimorph actuator with attached legs. The dynamic model of

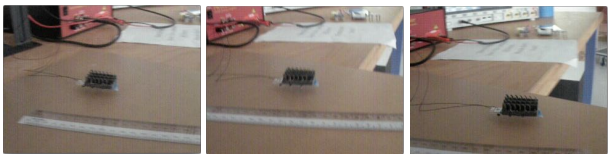

Fig. 9. Image sequence of the piezoelectric robot moving on a substrate.

the piezoelectric unimorph actuator is provided and the positions of legs are determined theoretically based on the dynamic model. A prototype of the piezoelectric mobile robot is fabricated and its locomotion behavior is experimentally verified. The speed versus applied voltage is reported on an acrylic substrate for bi-directional motion.

VII. Acknowledgement

The authors gratefully acknowledge the support of TL@SUTD-Systems Technology for Autonomous Reconnaissance & Surveillance and SUTD-MIT International Design Center (http://idc.sutd.edu.sg).

References

[1] Becker,F., Minchenya,V.,Zimmermann, K., and Zeidis, I. Single Piezo Actuator Driven Micro Robot for 2-Dimensional Locomotion. *Micromechanics and Microactuators, Springer*, 2012.

[2] Bernard, Y., Tian, Y., and Hernandez, C. Self moving Stick Slip piezoelectric actuator design and modelling. *Proceedings of piezo11, 27 February, Sestriere, Italy*, 2011.

[3] Cimprich, T., Kaegi, F., Driesen, W., et al. Ultrasonic monolithic piezoelectric multi DOF actuators for mobile microrobots. *Proceedings of ACTUATOR 06, Bremen, Germany*, 114–117, 2006.

[4] Uchino, K. Expansion from IT/Robotics to ecological/energy applications. *Proceedings of ACTUATOR 06, Bremen, Germany*, 48–54, 2006.

[5] Simu, U. and Jhansson, S. Fabrication of monolithic piezoelectric drive units for a miniature robot. *Journal of Micromechanics and Microengineering*,12(5):582-589, 2006.

[6] Ishihara, H., Fukuda, T., Kosuge, K., et al. Approach to distributed micro robotic systemdevelopment of micro line trace robot and autonomous micro robotic system. *IEEE international conference on robotics and automation, ICRA95, Nagoya, Japan, 2127 May*, 1995.

[7] Zesch, W., BYchi, R., Codourey, A., et al. Inertial drive for micro and nanorobots: two novel mechanics. *Proceedings in microrobotics and micromechanical systems, Philadelphia, PA, USA*, 2593:80-88, 1995.

[8] Hariri, H., Bernard, Y., and Razek, A. Locomotion principles for piezoelectric miniature robots. *Proceedings of ACTUATOR 10*,1015–1020, 2010.

[9] Uchino, K. Smart Materials and Structures, Piezoelectric ultrasonic motors: overview. *Smart Materials and Structures*,7:27–285, 1998.

[10] He, S., Chen, W., Tao, X. and Chen, Z. Standing wave bi-directional linearly moving ultrasonic motor. *IEEE Transactions on Ultrasonics, Ferroelectrics and Frequency Control*, 45(5):1133–1139, 1998.

[11] Roh, Y., Kwon, J. Development of a new standing wave type ultrasonic linear motor. *Sensors and actuators A*,112:196-202, 2004.

[12] Son, K. J., Kartik, V., Wickert, J. A., and Sitti, M. An Ultrasonic Standing-wave-actuated Nano-positioning Walking Robot: Piezoelectric-metal Composite Beam Modeling. *Journal of Vibration and Control*, 12:1293, 2006.

[13] Hariri, H., Bernard, Y., and Razek, A. Analytical and finite element model for unimorph piezoelectric actuator: Actuator design. *Proceedings of Piezo2011*, 71–75, 2011.

[14] R.G. Ballas, Piezoelectric multilayer beam bending actuator. *Springer*, 2007.

[15] Hariri, H., Bernard, Y., and Razek, A. A traveling wave piezoelectric beam robot. *Smart Materials and Structures*, 23(2), 2013.